Single and multisite graphene-based electroretinography recording electrodes: a benchmarking study

Jose de La Cruz, Diep Nguyen, Xavi Illa, Jessica Bousquet, Antonio Pérez-Marín, Elena del Corro, Serge Picaud, Jose Garrido, Clement Hebert

Single and multisite graphene-based electroretinography recording electrodes: a benchmarking study

Jose de la Cruz, Diep Nguyen, Xavi Illa, Jessica Bousquet, Antonio P. Pérez-Marín, Elena del Corro, Serge Picaud*, Jose A. Garrido*, Clement Hebert.

J. de la Cruz, Dr. J. Bousquet, A.P. Pérez, Dr. E. del Corro, Dr. C. Hebert, Prof. J. A. Garrido
Catalan Institute of Nanoscience and Nanotechnology (ICN2), CSIC and The Barcelona Institute of Science and Technology, Campus UAB, Bellaterra, 08193, Spain;

Dr. D. Nguyen, Prof. S. Picaud
Sorbonne Université, INSERM, CNRS, Institut de la Vision, France ;

Dr. X. Illa
Instituto de Microelectrónica de Barcelona IMB-CNM (CSIC), Esfera UAB, Bellaterra, 08193, Spain ;

Dr. X. Illa
Centro de Investigación Biomédica en Red en Bioingeniería, Biomateriales y Nanomedicina (CIBER-BBN), Madrid, 28029, Spain ;

Prof. J. A. Garrido
ICREA, Barcelona, 08010, Spain;
joseantonio.garrido@icn2.cat

Prof. S. Picaud
serge.picaud@inserm.fr

Keywords: graphene, ERG, MEA, photoreceptor degeneration

Electroretinography (ERG) is a clinical test employed to understand and diagnose many retinopathies. ERG is usually performed by placing a macroscopic ring gold wire electrode on the cornea while flashing light onto the eye to measure changes in the transretinal potential. However, macroscopic gold electrodes are severely limiting since they do not provide a flexible interface to contact the sensitive corneal tissue, making this technique highly uncomfortable for the patient. Another major drawback is the opacity of gold electrodes, that only allows them to record the ERG signal on the corneal periphery, preventing central ERG recordings. To overcome the limitations of metal-based macroscopic ERG electrodes, flexible electrodes are

fabricated using graphene as a transparent, flexible and sensitive material. The transparency of the graphene is exploited to fabricate micro-electrode arrays (MEA) able to perform multi-site recording on the cornea. The graphene-based ERG electrodes were benchmarked against the widely used gold electrodes in a P23H rat model with photoreceptor degeneration. This study shows that the graphene-based ERG electrodes can faithfully record ERGs under a wide range of conditions (light intensity, stage of photoreceptor degeneration, etc) while offering additional benefits for ERG recordings such as transparency and flexibility.

1. Introduction

Electroretinography is a technique that measures changes in the transretinal potential occurring when retinal cells activity changes as a response to a light stimulus. ERG is broadly used as a diagnostic test by clinicians to assess the functionality of different neurons of the retina.[1] This non-invasive technique involves placing an electrode on the cornea, flashing the eye with a controlled light, and recording the transretinal potential (see Figure 1a). ERG signals, so called electroretinograms, result from the synchronized multi-unit activity of retinal neurons responding to a defined light stimulation. Electroretinograms are composed of different components, each related to different cell types such that alterations in the expected shape of each component can be associated to specific retinopathies.[2]

The main components of an electroretinogram are the a-wave, the b-wave and the oscillatory potentials (OPS), as shown in Figure 1a. The a-wave is the first negative wave observed right after the light stimulus and it results from the hyperpolarization of the photoreceptors in the outer layers or the retina responding to the stimulus.[3,4] The b-wave is the positive wave occurring immediately after the a-wave, and represents the depolarization of ON bipolar cells. Finally, riding on the two waves, OPS represent fast oscillations between 100 and 150 Hz with an amplitude of few tens of μV which arise from the fast depolarization/hyperpolarization of the amacrine cells of the retina.[5,6]

The amplitude and latency of the a- and b-waves are defined by the local minimum and maximum of the ERG response, respectively. For a healthy animal under low-light levels, socalled scotopic conditions, the a-wave typically reaches its peak around few tens of milliseconds after stimulation, with an amplitude of few hundreds of μV. A delay/decrease in latency/intensity indicates a dysfunction in the phototransduction of the photoreceptors or photoreceptor loss.[7,8] Likewise, the b-wave is characterized by a latency of about 100 milliseconds and an amplitude of 1-2 mV, depending on the stimulus intensity and the type of electrode used to record the ERG.

Regarding the recording electrodes used for monitoring ERG, they can be divided in two categories: conjunctival and corneal electrodes.[9] A conjunctival electrode consists of a metal conductor, either a wire or a foil, bended in a way to make contact with the bulbar conjunctiva. Corneal electrodes, on the other hand, are prepared by bending a metal wire in a loop or attaching wires to a contact lens in order to place them over the surface of the cornea. Despite interfering with the central vision, their high signal amplitude make corneal electrodes the clinical standards.[10–12]

Both conjunctival and corneal electrodes present two important drawbacks: the discomfort produced by the rigid materials they are made of and the impossibility to measure signals from the whole cornea, since their opacity would block the light meant to stimulate the retina.

The opacity issue is especially troublesome since it hinders the use of MEA to record ERG. MEA technology is already the current state of the art in almost every field of bioelectronics and it has proven its ability to reliably record signals of very low amplitude, enable high density recordings[13,14] and even controlled stimulation capabilities with sub-mm spatial resolution.[15,16] Fully transparent MEA will allow for multi-site ERG recordings without blocking the light stimulus meant to stimulate the retina, providing local information of the cornea's electrical potential which could be used to trace local retinal pathologies.[17,18]

Therefore, electrodes made of a flexible and transparent material can offer novel solutions for ERG measurements.

Graphene, due to its high electrical conductivity and transparency, has become an attractive candidate for flexible and transparent electronics.[19] Due to its wide electrochemical potential window, relatively high interfacial capacitance and chemical stability in physiological conditions, single layer graphene SLG has also been extensively used for the detection of electrical cell signals in in vitro and in vivo studies.[20–22] Recently, graphene has also been successfully used to fabricate transparent and flexible electrodes for electroretinogram recordings.[9]

Here we set out to perform a systematic benchmarking of our flexible and transparent graphene electrodes against the current state of the art electrodes for ERG recordings. To do so we have used commercially available equipment aproved for clinical use to follow up a progressive photoreceptor degeneration in a P23H rat model. Despite previous groups having reported the use of transparent and flexible electrodes to record electroretrinograms[9], this is, to our best knwolede, the first attemp to use graphene electrodes to diagnose retinal degeneration, as well as the first benchmark against the clinical state of the art for animal recordingsFurthermore, we have fabricated graphene MEA to perform multi-site ERG recordings across the whole corneal surface. Regardless of other groups [17,18] taking this aproach, the limitations imposed by the oppacity of the used electrode material made necessary a complex PDMS well structure to separate the electrodes from the surface of the cornea. In that regard, graphene electrodes offer a better solution for multi-site ERG, since their transparency allows for better device integration.

2. Results and Discussion

2.1. Device design and characterization

Four different types of ERG electrodes have been used in this study. The first one is a commercial Au electrode made by bending a Au wire to create a toroidal electrode with an outer diameter of 3 mm and an inner diameter of 1.5 mm (Figure 1d). The second consists of a single layer graphene macroelectrode of 1 mm diameter covering the entire head of the probe (Figure 1b). The performance of these two designs is carefully compared in this study. Two other designs consisting of transparent MEA probes with 16 and 32 electrodes of 200 μm diameter have been investigated to assess their capability for multi-site ERGs (Figure 1c, Figure 3c and Figure 3d).

The graphene devices were fabricated using polyimide as a substrate on top of which titanium and gold tracks were evaporated. Then, the CVD grown graphene was transferred and patterned by reactive ion etching. Finally, the active area of the electrode was defined by passivating nonactive areas of the device using a second layer of photo-definable polyimide. In this way, it is ensured that no metal makes contact with the eye. The probes were then placed in a zeroinsertion force connector to interface the characterization and recording electronics. More details on the microfabrication procedures are provided in Materials and Methods.

After fabrication, the functionality of the devices was tested using electrochemical impedance spectroscopy (EIS) and by characterizing their noise performance. Figure 1e presents the Bode representation of the EIS. For all electrodes used in this study, the magnitude of the impedance is inversely proportional to the frequency (f) with values of 10^7, 10^6 and 10^4 Ohms at 100 Hz for the transparent MEA, the graphene single electrode and the gold electrode, respectively.

Regarding the phase, it stays close to -90 degrees in the investigated frequency range (0.5 to 300 Hz) for all electrodes. The Bode spectrum of the electrodes is close to that of a pure capacitor **(**Equation 1**)**,

$$Zc = \mathbf{1}/j\omega C \quad (1)$$

confirming the capacitive nature of the electrode-electrolyte interface.

Figure 1e also shows that the impedance of the commercial Au electrode is three orders of magnitude lower than that of the SLG graphene macroelectrode, meanwhile the difference between the impedance of the graphene MEA and the graphene macroelectrode is one order of magnitude. This difference can be easily explained considering the area of the electrodes: the area of the graphene microelectrodes is 0.03 mm^2 and the area of the macroelectrode is 0.785 mm^2. In the case of the Au ring electrode, its area is 44 mm^2.

In order to assess their ability to measure low amplitude signals, the intrinsic noise of the different electrodes has been studied. To this end, a baseline was recorded in absence of any external signal to measure the intrinsic noise of the system combining recording electrode and electronics. Then, the power spectral density (*PSD*) of the measured baseline was calculated, obtaining the corresponding electrode´s noise power at each frequency. In order to obtain the setup's floor noise the electrodes were removed from the recording setup, all their connections were grounded and a baseline recording was acquired to calculate the *PSD*. Figure 1f shows the *PSD* of the measured baseline recordings, depicted between 0.5 and 300 Hz, for the electrodes used in this study. At low frequencies, the difference in the noise power density for the graphene macro- and the micro-electrodes is about one order of magnitude and decreases at higher frequencies. Figure 1f also reveals that the noise power density of the Au electrode, the graphene macroelectrode and the floor noise of the recording setup remain practically the same over the whole frequency range, except at frequencies below 1 Hz. The *PSD* of a typical ERG recording is also shown in Figure 1f for comparison, demonstrating that the *PSD* noise level of the electrodes used in this study is well below the power of an ERG signal.

To understand the behaviour of the *PSD* signals of the electrodes used in this work we use the Johnson-Nyquist noise theory.[23] According to it, the voltage noise of an electrical conductor (V_n) is directly proportional to the square root of the impedance's real part of the conductor [*Re(Z)*],

$$V_n^2 = \mathbf{4}\, k_B T \int_{f1}^{f2} Re(Z) df \qquad (2)$$

with k_B the Boltzmann constant, T the temperature and f_1 and f_2 the frequencies that delimit the studied frequency band. From Equation 2, one might expect that the impedance difference between gold and graphene electrodes observed in Figure 1e would translate into a voltage noise difference; however, as shown in Figure 1f, this is not the case. To further quantify the experimentally observed noise, we can integrate the noise power density data shown in Figure 1f between 0.5 and 300 Hz, which yields a *Vn* of 4.9, 1.8 and 1.4 μV for the graphene microelectrodes, the graphene macroelectrode and the commercial Au electrode, respectively. We attribute the difference between the *PSD* of the noise baseline and what Johnson-Nyquist theory indicates to the contribution of the background noise of the recording setup (also shown in Figure 1f), which is the limiting factor for electrodes with low impedance and noise. Thus, the higher impedance of the graphene electrode does not hamper the quality of the recorded signal, having additional advantages such as its flexibility and transparency.

2.2. Retinitis Pigmentosa Diagnosis

In order to demonstrate the capabilities of the graphene electrode for the recording of ERGs, we chose the heterozygous P23H rat model. This rat line was created by incorporating a mutated rhodopsin gene on the wild-type Sprague Dawley rat, and is one of the most frequently used animal models for Retinitis Pigmentosa.[24–26] Its phenotype and genotype have been fully characterized[27] and they show a significantly slower retinal degeneration rate than the homozygous type.

For this study, full field ERG recordings were taken from P23H rats of 1, 2, 3, 5 and 7 months old under both scotopic (dark adapted) and photopic (light adapted) conditions to allow the study of rod and cone photoreceptor functions, respectively.[28] For the experiments, the animals were kept in the dark for at least 8 hours prior to the recording and handled under red light. The animals were then anesthetized and the ground and reference inserted on the back and the forehead respectively, as stated somewhere else.[18] For ERG recordings, the Au electrode and the graphene macroelectrode were used simultaneously, connecting each of them to one of the input channels of the commercial ERG system and placing each electrode on a different eye. The ERG recordings of all animals were obtained using the same graphene macroelectrode. For the stimulation, a Ganzfeld generator was used to provide white light stimulation accordingly to the ISCEV guidelines.[29] More details on the setup and the stimulation protocol are described in the Methods section.

Figure 2 shows the ERG obtained with the graphene macroelectrode and the commercial Au electrode on P23H rats of different ages and with different stimulation intensities, under scotopic (Figure 2a and b) and photopic (Figure 2d) conditions. The OPS, shown in Figure 2c, are obtained by band-pass filtering the data from the scotopic stimulation between 100 and 150 Hz.

Figure 2a shows the ERG recordings of the 1 month old rats obtained with different stimulation intensities under scotopic conditions, both for the graphene macroelectrode and the Au electrode. As expected, the amplitude of the a- and b-waves steadily increases with the stimulation intensity; the b-wave is already visible for intensities above $3 \cdot 10^{-6}$cd·s m^{-2}, and the a-wave at intensities above 10^{-4} cd·s m^{-2}. Furthermore, the signal-to-noise ratio (SNR) for the highest stimulation intensity reaches a value of 45 for both the gold and the graphene macroelectrode.

Focusing now on the time degeneration of photoreceptors, the retinal response appears normal for 1 month old rats under scotopic conditions (Figure 2b). However, a significant amplitude reduction of the a- and b-waves is already apparent for the 2 months old rats. The degeneration worsens with time, leading to the complete disappearance of the a-wave for 5 months old animals and an almost completely flat response at 7 months. Quantitatively, the comparison with the younger animals shows that at 2 months there is a 75% reduction (from -40 to -170 μV) of the a-wave amplitude, revealed by both the graphene and Au electrodes. In the case of the b-wave, both electrodes show the same reduction, of 50% (from 400 to 800 μV). We have also compared the latency of the b-wave for both electrodes. Using a stimulation intensity of 10 cd·s m^{-2}, we observed that the implicit time delay of the b-wave comparing the youngest (1 month old) with the oldest (7 months old) animals is close to 45 ms for both electrodes. The response of both electrodes can also be compared under photopic conditions. Figure 2d shows the a-wave suppression due to the light acclimatization; also, it reveals the expected decrease of the b-wave amplitude with time: 40% at month 2 and an almost completely flat response at month 7.

Figure 2c shows the OPS recordings for a stimulation intensity of 10 cd·s m^{-2} at three different ages (1, 2 and 3 months), also revealing the photoreceptor degeneration. From month 1 to 2 we observe a rapid increment in latency (10 ms) and a mild reduction in the signal amplitude (from 38 to 28 μV) taking the third OPS as a reference. From month 2 to month 3, we observe further degeneration; meanwhile the latency remains almost constant, a severe decrease in the signal makes the OPS disappear completely at ages older than 3 months.

Figure 2e summarizes the retinal degeneration on the amplitude of the a- and b-waves for the scotopic conditions and the b-wave for the photopic conditions. As stated before, the b-wave under photopic and scotopic conditions shows a steady degeneration. The b-wave amplitudes recorded the month 1 are close to 1 mV (scotopic) and 150 μV (photopic), and reach a value as

low as 50 μV (scotopic) and 10 μV (photopic) at month 7. The decay of the a-wave is more sudden, going from its initial 150 μV to a complete disappearance at month 3. Using a paired student t-test, there is no statistical difference for the b-wave amplitudes obtained with the graphene and gold, for any age. However, there is statistical significance difference for the awave amplitude recorded with graphene and Au electrodes at 5 months with stimulation of scotopic 10 ($p=0.005$), 3 ($p=0.03$), 0.3 cd·s m^{-2} ($p=0.007$), and 7 months with stimulation of scotopic 10 ($p=0.02$), and 3 cd·s m^{-2} ($p=0.009$). This is no surprise when we take into account that the a-wave normally disappears for P23H animals older than 5 months.[[27]] In this case, the amplitude of the signals is produced from the stochastic electrical noise of the system, that is uncorrelated between measurements.

Excluding the OPS recordings, where one particularly low signal increases the standard deviation for the Au electrode, the standard deviation of the ERG signals is larger for the graphene electrode than for the Au one. This is especially evident on the scotopic b-wave (Figure 2a and 2b). Since the noise of both electrodes is not that different (see Figure 1f), a possible explanation for this observation can be the electrode size. The graphene electrode is smaller than the Au one (1 mm vs 3 mm) and, consequently, it is more difficult to position it on the same place from animal to animal. This position difference could result in more uncertainty in the recording of the signal amplitude, as will be discussed in the next section.

All in all, these findings confirm the good performance of the single graphene electrode: it is not only flexible, transparent and smaller than the Au electrode, but it also allows to record a faithful ERG signal that accurately reflects the photoreceptor degeneration of the P23H rat model, exhibiting a similar SNR than the commercial Au electrode.

2.1. ERG Recordings with MEA

One of the advantages of graphene as a material to fabricate ERG recording electrodes is its transparency. As opposed to the conventionally used metallic conductors, graphene transparency allows to fabricate MEAs able to record with multiple sites from the whole surface of the cornea without blocking the light stimulus. Multisite recordings can provide local information on the corneal electrical potential, which could eventually be used to obtain information of local retinal deficiencies.[18]

Currently, multifocal ERG (mf-ERG) is the preferred diagnostic technique to provide topographical information of retinal activity. When performing mf-ERG, a pattern, instead of a light flash, is presented to the patient`s eye and the signal coming from the different parts of the retina is recorded from the whole surface of the cornea with only one macroscopic electrode. With MEA ERG, in contrast, information from different regions of the retina could be extracted with only one stimulation flash.[17,18] This could allow physicians to get topographical measurements of retinal activity in a faster and, potentially, more comfortable way.

To demonstrate the capabilities of graphene-based MEA ERG devices, we fabricated transparent MEA ERG probes with two different designs, as shown in Figures 3c and d. Both designs consist of arrays of 200 μm diameter transparent graphene electrodes, in which part of the metal tracks have been substituted by transparent graphene tracks; the width-to-length ratio of the transparent graphene tracks has been tailored in order to prevent big variations in track resistance for different electrodes. The first device is a probe with 16 electrodes linearly distributed; it consists of a finger design in which the supporting polyimide is structured in such a way that allows independent movement of each of the electrodes, facilitating the microelectrodes to conform to the spherical shape of the cornea, as shown in Figure 1c. The second design consists of 31 electrodes distributed in a hexagonal pattern, with higher electrode density towards the centre, such as those used to stimulate and record electrical activity in the

retina.[30] The supporting polyimide structure has openings that allow for the tear film covering the cornea to pass through, ensuring a closer contact between the electrodes and the corneal surface; the openings in the polyimide structure also improve the flexibility of the head of the probe.

Figure 3 shows several ERG recordings performed with the two different graphene MEA designs described above. The shown ERG data correspond to the average of 20 flashes, each with an intensity of 10 cd·s m^{-2}. In this way, the SNR can be compared to data obtained with the big electrodes and shown in Figure 2, where the data is an average of 5 flashes over 4 different animals. Figure 3a shows a mapping of the corneal potential performed with the circular MEA; the location of the signals in the figure corresponds with the position of the electrodes on top of the cornea. Figure 3e shows an ERG map obtained with the linear MEA probe, positioned on the cornea along the nasal-temporal direction, as depicted in the schematic in the figure. Figure 3b shows two ERGs recorded by an electrode in a circular probe (in blue) and an electrode on a linear probe (in red). A band pass filter applied between 100 and 150 Hz allow us to further see the details and the characteristic shape of the OPS, demonstrating that all ERG features are perfectly captured by the transparent MEA probes with graphene microelectrodes.

MEA ERG recordings have been previously used to characterize spatial differences on the corneal potential[17] or to locate induced injuries on the retina.[18] In these studies, however, the density of integration and size of the electrodes was limited by the opacity of the sensing material and for the shadows the electrodes cast on the retina, blocking in some cases up to 35% of the stimulation flash.[17] Another limitation of prior studies was the placement of the electrodes since they had to be moved away and connected to the cornea through an intricate PDMS well system in order to minimize the effect of the distorted wave front by the diffraction pattern of the opaque electrodes.

In light of these challenges we set out to use our MEA ERG to detect lesions on the retina. For that purpose, we induced a lesion in the temporal-ventral quadrant of the retina of 10 male Long Evans rats following the protocol described in the Methods section. After the lesion was induced the animals were allowed to recover for a minimum period of 7 days and then the ERG signals were recorded using both types of MEAs probes and the same protocol described in Figure 3. For illustrative purposes, Figure S3 shows a particular example of an ERG measured with the linear MEA in which the electrodes in the nasal position record a significantly lower b-wave amplitude than the rest of the electrodes. However, the variability in the injury size and position, the natural variability of the ERG signal among different animals, the lack of a robust method to ensure the reproducible placement of the electrode from rat to rat and the small nature of the differences we were looking for (reported to be less than 3%[31]) made impossible to confidently and systematically extract the position of the injury from the ERG signal differences measured with our MEA probes. . Our results indicate that more work needs to be dedicated to understand how this new tool can be used to expand our understanding of the topography of ERGs in the cornea.

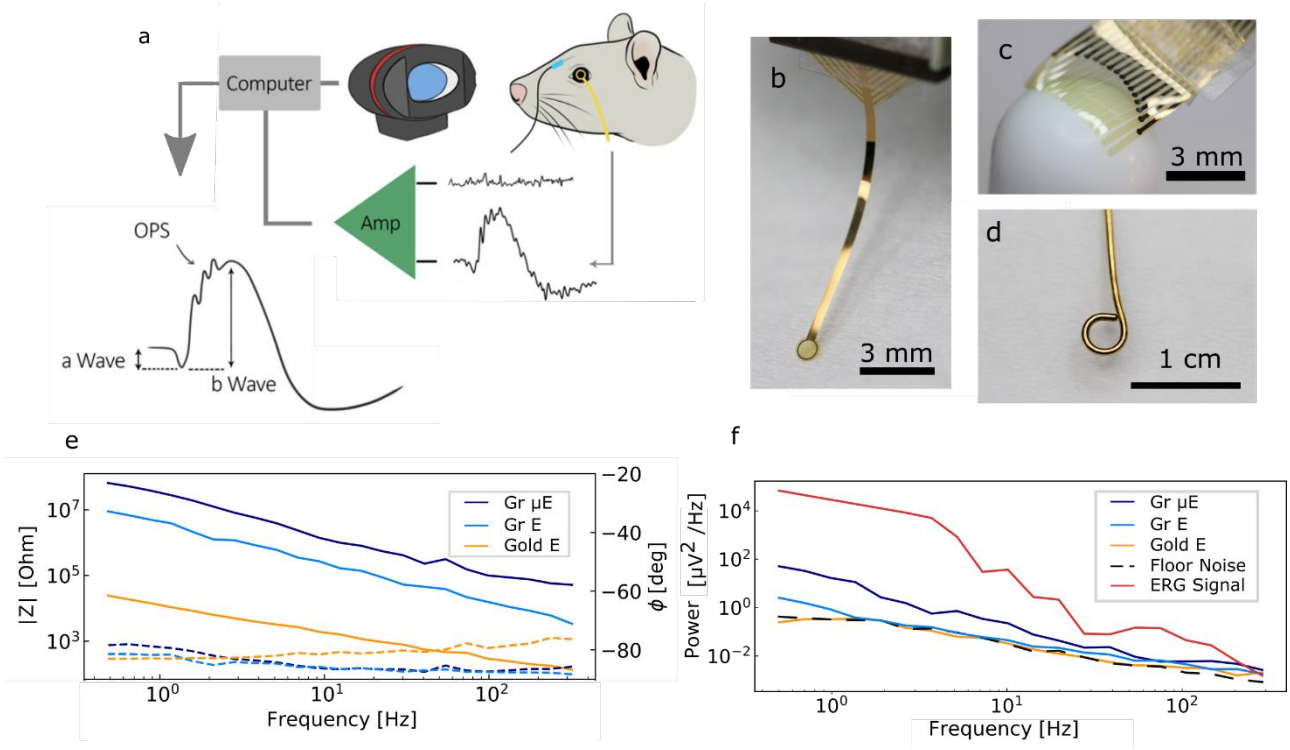

Figure 1. ERG recording setup, ERG electrodes and their characterization. a) Schematic representation of the ERG experiments. A Ganzfeld stimulator illuminates the eye of the rodent and the signal from the retina is recorded with a graphene electrode. The recorded signal is subtracted from that of a reference electrode placed on the forehead and amplified with an operation amplifier. b) Flexible probe containing a graphene macroelectrode, of 1 mm diameter. c) Image of a linear-type microelectrode array (MEA) probe showing how the finger-like design allows the individual electrodes to conform to a spherical shape. d) Image of a Au electrode, which is current state of the art for ERG recording in rodents. e)-f) Electrical characterization of the graphene MEA (Gr µE), graphene macroelectrode (Gr E) and Au electrode (Au E). e) Electrochemical Impedance Spectroscopy Bode plot of the graphene and gold electrodes used in this study. Solid lines denote the module |Z| of the impedance and dashed lines the phase. f) Power spectral density (*PSD*) of a noise baseline measured with the same electrodes shown in e); it also shows the *PSD* of the background noise of the recording setup with the amplifier channels connected to ground and the *PSD* of a typical ERG signal.

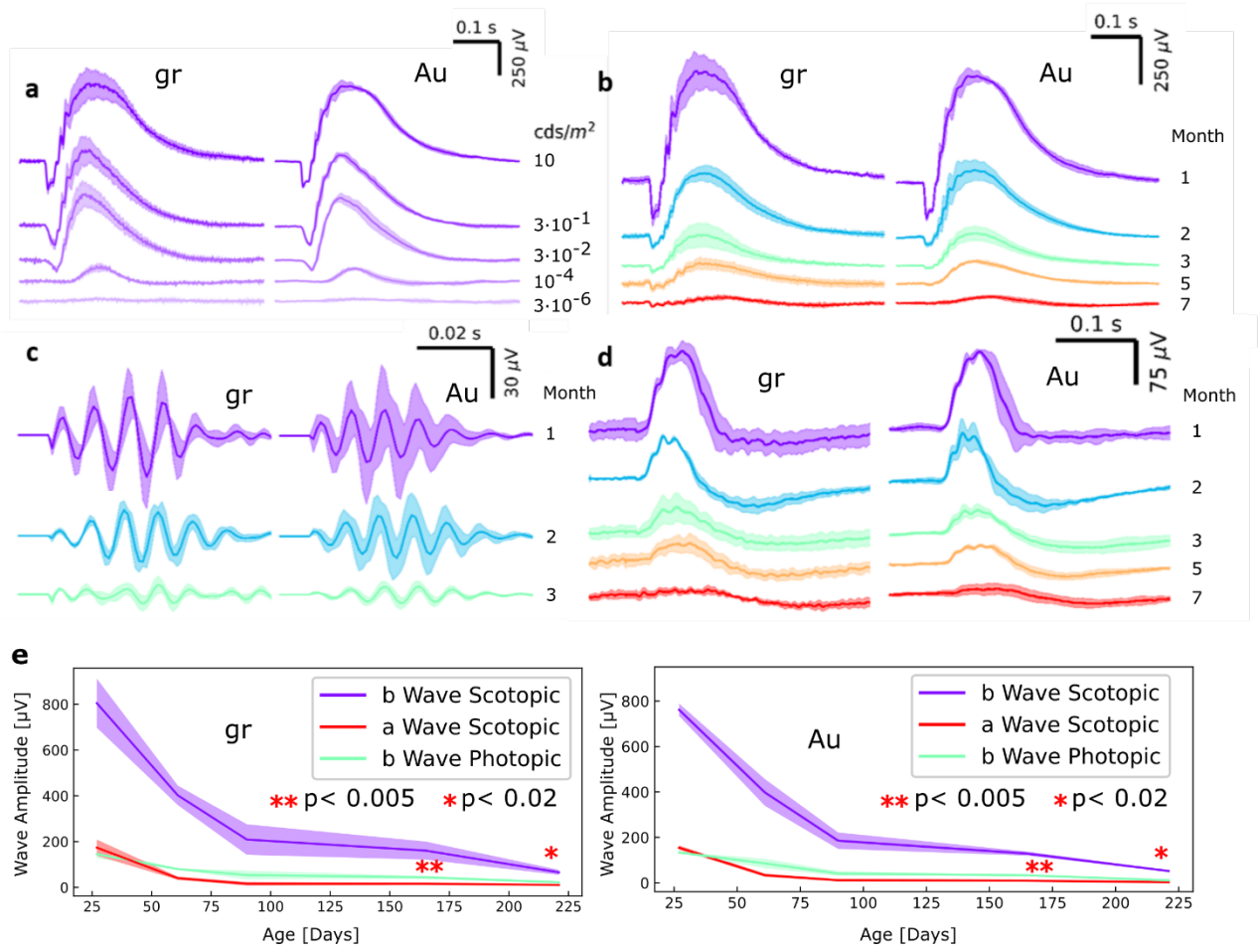

Figure 2. Comparison of the ERG recordings between the graphene macroelectrode and a commercial Au electrode on P23H degenerating rats under scotopic and photopic conditions. The results are the averages over 4 different animals, represented by the solid line. The shaded area represents the standard deviation of each measurement. a) ERG recorded under different stimulation intensities (ranging from 10 to $3 \cdot 10^{-6}$ cd·s m^{-2}) in 27 days old rats under scotopic conditions. b) ERG recorded in animals of different ages using a stimulation of 10 cd·s m^{-2} intensity under scotopic conditions. c) Oscillatory Potentials (OPS) under scotopic conditions for animals 1, 2 and 3 months old. d) ERG recorded in animals of different ages with 10 cd·s m^{-2} stimulation intensity under photopic conditions. e) Maximum amplitude of the scotopic awave and b-wave and photopic b-wave recorded with the graphene macroelectrode (left) and a commercial Au electrode (right) with a stimulation intensity of 10 cd·s m^{-2}.Statistical analysis showed that graphene recorded significantly higher a-wave amplitudes for the 5 (**p

< 0.005) and 7 (* p < 0.02) months (n=4). The shaded area represents the standard deviation of each set of measurements. For convenience, the absolute value of the a-wave is presented.

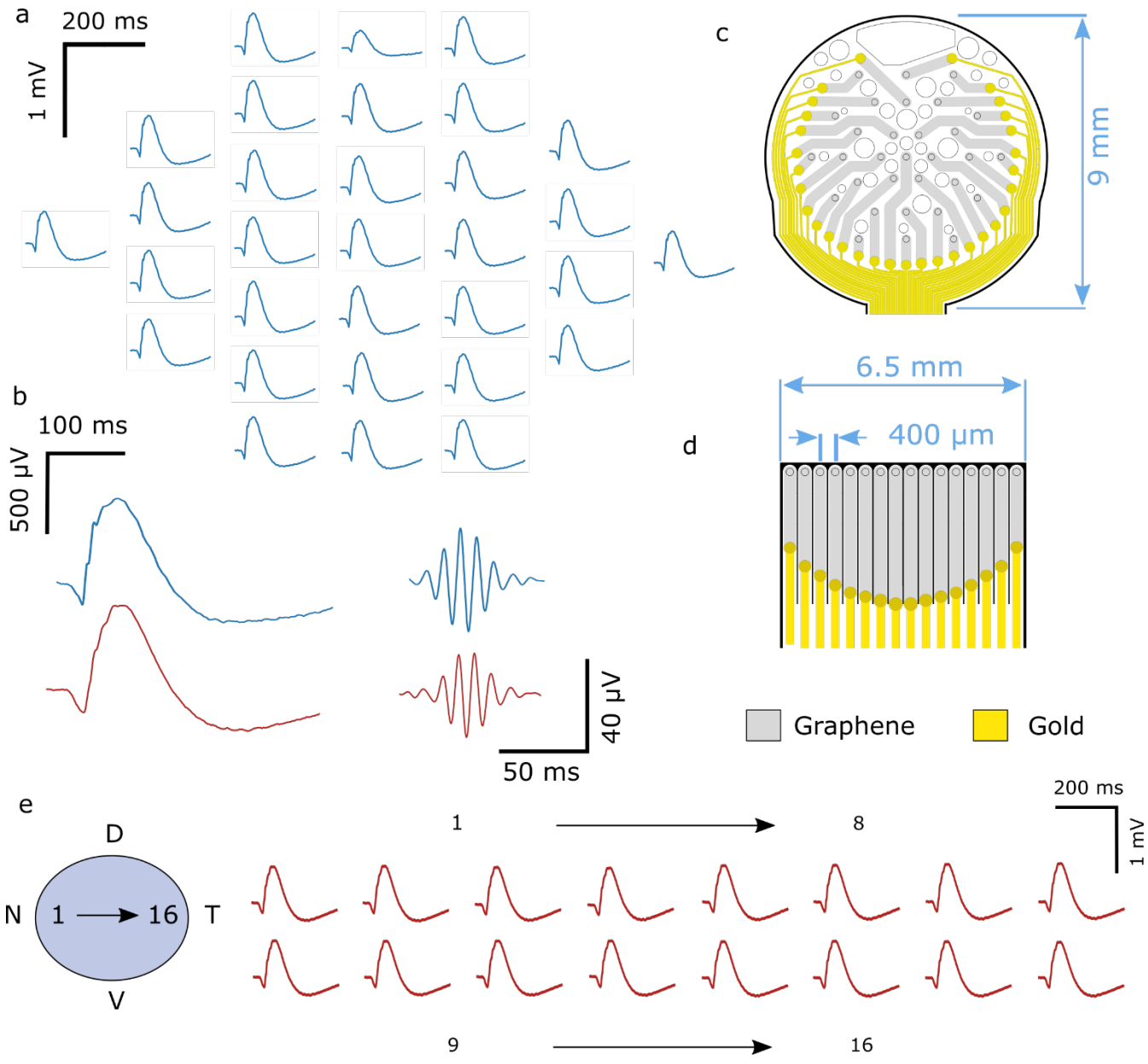

Figure 3. ERG recordings with transparent graphene MEA probes. a) Mapping of the corneal potential performed with the circular MEA. The distribution of the signals in the figure corresponds with the position of the electrodes on top of the cornea. The data shown is an average of 20 flashed at 10 cd s/m² stimulation intensity under scotopic conditions and filtered between 0.5 and 300 Hz. b) Close-up of representative ERG signals measured with the

circular probe (blue) and the linear probe (red). Also shown OPS signals acquired applying an additional bandpass filter between 100 and 150 Hz. c-d) Design specifications of the circular and linear probes used in this study. e) Mapping of the corneal potential performed with the linear MEA; the schematic indicates the position of the electrodes on the cornea. Electrodes number 1 and 16 are in the nasal and temporal position, respectively. Stimulation intensity, averaging and filtering are the same used in part a.

3. Conclusion

Selecting an adequate material for the fabrication of an ERG electrode is the first step for successful and reliable recordings. When choosing the material, several considerations have to be kept in mind; firstly, the material has to be sensitive enough to changes in potential to record the electrical signal produced by the retina; secondly, the chosen material should not disturb the light used to stimulate the retina; thirdly, it has to be chemically stable under biological conditions since it is going to be in direct contact with the cornea; and finally, the material has to be flexibe, in order to conform properly to the eye and to facilitate as much as possible the data acquisition. Given its sensibility, transparency, stability in biological conditions and flexibility, graphene is an exceptional candidate for the fabrication of ERG electrodes. In this study, we have benchmarked the performance of our flexible and transparent graphene electrodes against the current state of the art for ERG recording using the P23H animal model of photoreceptor degeneration. As expected, drastic vision loss is observed at the 60-day mark represented by the diminished amplitude in the a- and b scotopic waves, the OPS and the b photopic wave. We have also proved that the ERG measurements performed with the graphene single electrode are not statistically different than those measured with the commercial Au electrode, confirming that our flexible and transparent graphene electrodes are perfectly suited to diagnose photoreceptor degeneration.

Additionally, in this work, we have exploited the graphene transparency to fabricate MEA with potential to provide topographical information of retinal activity with sub-mm spatial resolution. We have shown that the ERG MEA are perfectly able to faithfully record the characteristic features of ERG such as the a- and b-waves and the OPS. In this study, we have also attempted to use our MEA ERG to detect induced lesions on the retina. However, due to the natural variability of the ERG signal from animal to animal and technical factors like the precise placement of the electrode and injury reproducibility, our results are not conclusive.

More work needs to be devoted to fully exploit the advantages of graphene MEA for ERG recordings. Specifically, accurate simulations[31] and the use of novel MEA encapsulation materials[32] could eventually pave the way to locate retinal injuries using topographical information of the corneal potential provided by MEAs.

Altogether, our study confirms that graphene, with its flexibility, transparency, and sensing capability, is an excellent material for ERG recording. In addition, graphene technology provides the capability to fabricate flexible and transparent arrays with multiple electrodes, offering novel opportunities to explore yet unexploited aspects of electroretinography.

4. Methods

4.1. Graphene growth and device fabrication

CVD graphene is grown on 25 μm thick copper foil. Prior to the growth, copper is electropolished, cleaned with isopropanol and placed on a hot wall reactor where it is annealed before the graphene growth is carried out, as stated elsewhere.[33]

The whole photolithography fabrication process is carried out on four-inches silicon wafers, on which a layer polyimide (PI-2611, HD MicroSystems) is spin coated to serve as a substrate. After the hard bake, the lithography of the metal tracks is done using a negative resist (AZ5241E Clariant) and a layer of metal (Ti/Au, 20/200 nm) is evaporated. Following the lift off of the resist, single layer graphene is transferred by means of a wet etching technique. A second

lithography step (HiPR 6512, Fuji Film) is then performed to define the active area of the devices etching away the excess graphene by means of oxygen reactive ion etching. Then the polyimide substrate is structured using reactive ion etching and layer of AZ9620 resist as mask. Finally, the devices are passivated using the permanent positive resist HD8820 and peeled off from the wafer. More details about the fabrication have been reported elsewhere.[33,34]

4.2. Device characterization

The devices were individually characterized by performing impedance spectroscopy (BioLogic SP-200) in a three-electrode configuration with a platinum foil as the counter electrode and an Ag/AgCl (Dry FlexRef, WPI) reference electrode, in a 500 mM PBS solution. The floor noise of the electrode was measured (OpenEphys Acquisition board with Intan RHD2132 amplifier board) by integrating the Power Spectral Density (*PSD*) between 0.5 and 300 Hz using a custom-made Python code.

4.3. Animal Model

The P23H rat is a model of rod-cone retinal degeneration developed by the transfection of a mutated RHO gene encoding for rhodopsin protein. The heterozygous P23H model is generated by cross breeding homozygous transgenic P23H donated from the laboratory of Matthew LaVail from USCF School of Medicine with wild-type albino Sprague-Dawley rats purchased from Janvier Labs (France). ERGs recorded with MEAs were performed on healthy Long Evans adult rats of 2 months. Animals were housed by enclosure in a controlled environment with a half-day dark/light cycle with nutrition ad libitum. All procedures were carried out in accordance to the guidelines of the European community council directive (86/609/EEC) and approved by the Charles Darwin No5 Ethics Committee in Animal Experimentation (agreement #15219).

Animals were allowed for dark adaptation of 8 hours prior to recordings and all handling was done under red light. Fixed anaesthesia was delivered using a mix of ketamine (60 mg kg^{-1}

Imalgene1000, Merial, FR) and medetomidine (0.4 mg kg^{-1} Domitor, Pfizer, Sante) diluted in NaCl solution (B. Braum Medical, FR) and administered via intraperitoneal injection. A heating platform maintained body temperature throughout the recording. Tropicamide 0.5 % drops (Laboratoires Théa, FR) were used for eye dilatation and oxybuprocaine chlorhydrate 0.4 % drops (Bausch & Lomb, CAN) were used to provide local anaesthesia of the cornea. Ocular gel (Dechra Pharmaceuticals, UK) maintained eye hydration throughout the experiment that lasted under 45 minutes.

4.4. ERG recording

Scotopic recordings used white light stimulation of intensities $3.0 \cdot 10^{-6}$, $3.0 \cdot 10^{-5}$, 10^{-4}, 0.03, 0.3, 3, and 10 cd s m^{-2} Each intensity had 5 flashes of 4 ms every 20 s. Photopic recordings required 5 min of light adaptation in 20 cd s m^{-2} white light before light stimulation. 10 flashes of 4 s at 10 cd s m^{-2} with background adapted light were delivered with 30 s between each flash. Electrodes were placed at the center of the cornea and enveloped in ocular gel. The OPS signals for the youngest animal appear to be different when measured with the graphene and the gold electrodes, with 45 μV and 31 μV peak to peak signal amplitude respectively. Despite this apparent difference, the large standard deviation of the OPS signals recorded with the gold electrode are caused by one of the measurements being particularly low. This large standard deviation implies that there is no significant difference between both signals ($p = 0.55$, student t-test).

For the graphene macroelectrode and the gold electrode, raw data was acquired with a commercial ERG system; E3 Desktop, Diagnosys, Illinois. The stimulation was performed with a Ganzfeld generator (ColorDome Binocular Flash Stimulator, Diagnosys, Illinois). For the graphene MEA, the data was acquired with an OpenEphys Acquisition board together with an Intan RHD2132 amplifier board. The stimulation was achieved with a collimated white LED light (MWWHL4 from Thorlabs, powered by a stimulus generator (STG-4002, Multi-Channel Systems GmbH) calibrated to deliver a 10 cd s m^{-2} light stimulus and duration of 4 ms.

4.5. Lesion study

To induce a lesion in the temporal-ventral quadrant of the retina, a 532 nm laser pulse with 500 mW power and 100 ms duration was used. Prior to this procedure the animals were anesthetized using the same protocol described for the ERG recordings (60 mg kg^{-1} ketamine and 0.4 mg kg^{-1} Domitor).

4.6 Statistical Analysis

The analysis to determine if the values recorded by the graphene and the gold electrodes are statistically different was done using a two sided Student´s t test for the null hypothesis that both populations (n = 4) had identical average. We used a custom code written in Python 3.6 and the function ttest_ind from the Scipy library.

Acknowledgements

This project has received funding from the European Union's Horizon 2020 research and innovation programme under grant agreement No. 785219 (GrapheneCore2), No. 881603 (GrapheneCore3) and No. 732032 (Braincom). This work is within the project FIS2017-85787-R funded by the "Ministerio de Ciencia, Innovación y Universidades" of Spain, the "Agencia Estatal de Investigación (AEI)", and the "Fondo Europeo de Desarrollo Regional (FEDER/UE)". Support was also provided by the French state funds managed by the Agence Nationale de la Recherche within the Programme Investissements d'Avenir, LABEX LIFESENSES [ANR-10-LABX-65] and IHU FOReSIGHT [ANR-18-IAHU-0001]. The ICN2 is supported by the Severo Ochoa Centres of Excellence program, funded by the Spanish Research Agency (AEI, grant no. SEV-2017-0706), and by the CERCAProgram/Generalitat de Catalunya. EDC acknowledges the Spanish MINECO Juan de la Cierva Fellowship JC-201525201.

This work has made use of the Spanish ICTS Network MICRONANOFABS partially supported by MICINN and the ICTS 'NANBIOSIS', more specifically by the Micro-NanoTechnology Unit of the CIBER in Bioengineering, Biomaterials and Nanomedicine (CIBER-BBN) at the IMB-CNM.

Jose de la Cruz would like to thank Laura García for the work on the images and figures throughout the whole paper writting process.

J. C. and D. N. contributed equally to this work.

Received: ((will be filled in by the editorial staff))
Revised: ((will be filled in by the editorial staff))
Published online: ((will be filled in by the editorial staff))

References

[1] L. Xu, S. L. Ball, K. R. Alexander, N. S. Peachey, *Vis. Neurosci.* **2003**, *20*, 297.

[2] A. E. Weymouth, A. J. Vingrys, *Prog. Retin. Eye Res.* **2008**, *27*, 1.

[3] K. Brown, M. Murakami, *Nature* **1964**, *201*, 626.

[4] K. T. Brown, T. N. Wiesel, *J. Physiol.* **1961**, *158*, 257.

[5] P. Speros, J. Price, *Surv. Ophthalmol.* **1981**, *25*, 237.

[6] D. Yonemura, K. Kawasaki, *Doc. Ophthalmol.* **1979**, *48*, 163.

[7] E. Tan, Q. Wang, A. B. Quiambao, X. Xu, N. M. Qtaishat, N. S. Peachey, J. Lem, S. J. Fliesler, D. R. Pepperberg, M. I. Naash, M. R. Al-Ubaidi, *Investig. Ophthalmol. Vis. Sci.* **2001**, *42*, 589.

[8] N. Cuenca, I. Pinilla, Y. Sauvé, R. Lund, *Eur. J. Neurosci.* **2005**, *22*, 1057.

[9] R. Yin, S. Zhao, X. Meng, H. Peng, X. Duan, Z. Xu, Z. Liu, M. K. Priydarshi, Y. Liu, Z. Chen, B. Deng, K. Wang, T. Tang, M. Mei, *Nat. Commun.* **2018**, *9*, DOI 10.1038/s41467-018-04781-w.

[10] L. Esakowitz, A. Kriss, F. Shawkat, *Doc. Ophthalmol.* **1993**, 169.

[11] M. Gjötterberg, *Arch. Ophthalmol.* **1986**, *104*, 569.

[12] F. Carpi, F. Tomei, *Biomed. Pharmacother.* **2006**, DOI 10.1016/j.biopha.2006.07.002.

[13] D. Khodagholy, J. N. Gelinas, T. Thesen, W. Doyle, O. Devinsky, G. G. Malliaras, G. Buzsáki, *Nat. Neurosci.* **2015**, *18*, 310.

[14] M. Ballini, J. Muller, P. Livi, Y. Chen, U. Frey, A. Stettler, A. Shadmani, V. Viswam, I. L. Jones, D.

Jackel, M. Radivojevic, M. K. Lewandowska, W. Gong, M. Fiscella, D. J. Bakkum, F. Heer, A. Hierlemann, *IEEE J. Solid-State Circuits* **2014**, *49*, 2705.

[15] M. Jole, I. A. Leccardi, N. Aurelia, L. Chenais, L. Ferlauto, M. Kawecki, E. Geneviève Zollinger, D. Ghezzi, **n.d.**, DOI 10.1038/s43246-020-0023-4.

[16] S.-M. Kim, N. Kim, Y. Kim, M.-S. Baik, M. Yoo, D. Kim, W.-J. Lee, D.-H. Kang, S. Kim, K. Lee, M.H. Yoon, *NPG Asia Mater.* **2018**, *10*, 255.

[17] Y. Krakova, H. Tajalli, S. Thongpang, Z. Derafshi, T. Ban, S. Rahmani, A. N. Selner, A. Al-Tarouti, J. C. Williams, J. R. Hetling, *Doc. Ophthalmol.* **2014**, *129*, 151.

[18] Z. Derafshi, B. E. Kunzer, E. M. Mugler, N. Rokhmanova, D. W. Park, H. Tajalli, K. Shetty, Z. Ma, J. C. Williams, J. R. Hetling, *Investig. Ophthalmol. Vis. Sci.* **2017**, *58*, 2863.

[19] A. C. Ferrari, F. Bonaccorso, V. Fal'ko, K. S. Novoselov, S. Roche, P. Bøggild, S. Borini, F. H. L. Koppens, V. Palermo, N. Pugno, J. A. Garrido, R. Sordan, A. Bianco, L. Ballerini, M. Prato, E. Lidorikis, J. Kivioja, C. Marinelli, T. Ryhänen, A. Morpurgo, J. N. Coleman, V. Nicolosi, L. Colombo, A. Fert, M. Garcia-Hernandez, A. Bachtold, G. F. Schneider, F. Guinea, C. Dekker, M. Barbone, Z. Sun, C. Galiotis, A. N. Grigorenko, G. Konstantatos, A. Kis, M. Katsnelson, L. Vandersypen, A. Loiseau, V. Morandi, D. Neumaier, E. Treossi, V. Pellegrini, M. Polini, A. Tredicucci, G. M. Williams, B. Hee Hong, J. H. Ahn, J. Min Kim, H. Zirath, B. J. Van Wees, H. Van Der Zant, L. Occhipinti, A. Di Matteo, I. A. Kinloch, T. Seyller, E. Quesnel, X. Feng, K. Teo, N. Rupesinghe, P. Hakonen, S. R. T. Neil, Q. Tannock, T. Löfwander, J. Kinaret, *Nanoscale* **2015**, *7*, 4598.

[20] B. M. Blaschke, N. Tort-Colet, A. Guimerà-Brunet, J. Weinert, L. Rousseau, A. Heimann, S. Drieschner, O. Kempski, R. Villa, M. V. Sanchez-Vives, J. A. Garrido, *arXiv* **2016**, DOI 10.1088/2053-1583/aa5eff.

[21] C. Hébert, E. Masvidal-Codina, A. Suarez-Perez, A. B. Calia, G. Piret, R. Garcia-Cortadella, X. Illa, E. Del Corro Garcia, J. M. De la Cruz Sanchez, D. V. Casals, E. Prats-Alfonso, J. Bousquet, P. Godignon, B. Yvert, R. Villa, M. V. Sanchez-Vives, A. Guimerà-Brunet, J. A. Garrido, *Adv. Funct. Mater.* **2018**, *28*, 1.

[22] E. Masvidal-Codina, X. Illa, M. Dasilva, A. B. Calia, T. Dragojević, E. E. Vidal-Rosas, E. PratsAlfonso, J. Martínez-Aguilar, J. M. De la Cruz, R. Garcia-Cortadella, P. Godignon, G. Rius, A.
Camassa, E. Del Corro, J. Bousquet, C. Hébert, T. Durduran, R. Villa, M. V. Sanchez-Vives, J. A. Garrido, A. Guimerà-Brunet, *Nat. Mater.* **2019**, *18*, DOI 10.1038/s41563-018-0249-4.

[23] J. B. Johnson, *Phys. Rev.* **1927**, *541*.

[24] L. Fernández-Sánchez, G. Esquiva, I. Pinilla, P. Lax, N. Cuenca, *Front. Neuroanat.* **2018**, *12*, 1.

[25] D. Y. Yu, S. Cringle, K. Valter, N. Walsh, D. Lee, J. Stone, *Investig. Ophthalmol. Vis. Sci.* **2004**, *45*, 2013.

[26] L. Fernández-Sánchez, P. Lax, C. Isiegas, E. Ayuso, J. M. Ruiz, P. De La Villa, F. Bosch, E. J. De La Rosa, N. Cuenca, *Hum. Gene Ther.* **2012**, *23*, 1290.

[27] E. Orhan, D. Dalkara, M. Neuillé, C. Lechauve, C. Michiels, S. Picaud, T. Léveillard, J. A. Sahel, M. I. Naash, M. M. LaVail, C. Zeitz, I. Audo, *PLoS One* **2015**, *10*, 1.

[28] G. B. J. Keiner, in *Webvision Organ. Retin. Vis. Syst.*, **2001**, pp. 76–80.

[29] D. L. McCulloch, M. F. Marmor, M. G. Brigell, R. Hamilton, G. E. Holder, R. Tzekov, M. Bach, *Doc. Ophthalmol.* **2015**, *130*, 1.

[30] G. D. Field, J. L. Gauthier, A. Sher, M. Greschner, T. A. MacHado, L. H. Jepson, J. Shlens, D. E. Gunning, K. Mathieson, W. Dabrowski, L. Paninski, A. M. Litke, E. J. Chichilnisky, *Nature* **2010**, *467*, 673.

[31] A. N. Selner, Z. Derafshi, B. E. Kunzer, J. R. Hetling, *IEEE Trans. Biomed. Eng.* **2018**, *65*, 2781.

[32] C. M. Tringides, N. Vachicouras, I. de Lázaro, H. Wang, A. Trouillet, B. R. Seo, A. EloseguiArtola, F. Fallegger, Y. Shin, C. Casiraghi, K. Kostarelos, S. P. Lacour, D. J. Mooney, *Nat. Nanotechnol.* **2021**, DOI 10.1038/s41565-021-00926-z.

[33] R. Garcia-Cortadella, E. Masvidal-Codina, J. M. De la Cruz, N. Schäfer, G. Schwesig, C. Jeschke, J. Martinez-Aguilar, M. V. Sanchez-Vives, R. Villa, X. Illa, A. Sirota, A. Guimerà, J. A. Garrido, *Small* **2020**, *16*, 1.

[34] N. Schaefer, R. Garcia-Cortadella, A. B. Calia, N. Mavredakis, X. Illa, E. Masvidal-Codina, J. de la Cruz, E. del Corro, L. Rodríguez, E. Prats-Alfonso, J. Bousquet, J. Martínez-Aguilar, A. P. PérezMarín, C. Hébert, R. Villa, D. Jiménez, A. Guimerà-Brunet, J. A. Garrido, *Carbon N. Y.* **2020**, *161*, 647.

Graphene electrodes and graphene microelectrode arrays are a promising alternative to the current state of the art in the field of electroretinogram (ERG) recording. The graphene electrodes shown in this study are able perform ERG recordings with similar signal to noise ratio (SNR) as the widely used gold electrodes; providing additional benefits such as transparency and flexibility.

Jose de la Cruz, Diep Nguyen, Xavi Illa, Jessica Bousquet, Antonio P. Pérez, Elena del Corro, Serge Picaud*, Jose A. Garrido*, Clement Hebert.

Single and multisite graphene-based electroretinography recording electrodes: a benchmarking study